RSC Advances

This is an *Accepted Manuscript*, which has been through the Royal Society of Chemistry peer review process and has been accepted for publication.

Accepted Manuscripts are published online shortly after acceptance, before technical editing, formatting and proof reading. Using this free service, authors can make their results available to the community, in citable form, before we publish the edited article. This *Accepted Manuscript* will be replaced by the edited, formatted and paginated article as soon as this is available.

You can find more information about *Accepted Manuscripts* in the Information for Authors.

Please note that technical editing may introduce minor changes to the text and/or graphics, which may alter content. The journal's standard Terms & Conditions and the Ethical guidelines still apply. In no event shall the Royal Society of Chemistry be held responsible for any errors or omissions in this *Accepted Manuscript* or any consequences arising from the use of any information it contains.

ROYAL SOCIETY OF CHEMISTRY

www.rsc.org/advances

Hierarchical Ni-Felayered double hydroxide/MnO_2 spherearchitecture as an efficient noble metal-free electrocatalyst for ethanol electro-oxidation in alkaline solution

ZhijunJia, Yi Wang*, Tao Qi

National Engineering Laboratory for Hydrometallurgical Cleaner Production Technology, Institute of Process Engineering, Chinese Academy of Sciences, Beijing 100190, China

**Corresponding authors: Y. Wang, Fax: (+86) 10 82544848-802, Tel: (+86) 10 82544967, E-mail: wangyi@ipe.ac.cn*

Abstract: Ni-Fe layered double hydroxide (LDH) nanosheets and hierarchical Ni-Fe LDH@MnO_2 spheresare synthesized by a facile and cost-effective approach for highly efficient ethanol electro-oxidation. The LDH@MnO_2 microsphere displays excellent catalytic activity and robust durability for ethanol electro-oxidation, compared with the Ni-Fe LDHnanosheets. According to the analyses for nitrogen adsorption isotherms and electrochemical impedance spectra (EIS), it is inferred that the performance enhancing could be attributed to that MnO_2 could increase the concentration of OH_{ads}species on Ni-Fe LDH surface and these OH_{ads}can react with C_{1ad} intermediate species to produce CO_2 or water soluble products, releasing the active sites on LDH for further electrochemical reaction. Therefore, it is expected that an effective noble-metal free catalysts for ethanol electro-oxidation could be obtained by tailoring structure and properties of LDHs and their composites.

Keywords: Ni-Fe LDH; MnO_2; Ethanol; Electro-oxidation; Electrocatalyst

RSC Advances Accepted Manuscript

Introduction

Considerable efforts have been fueled up to exploit green, sustainable and efficient power sources owning to the increasing global demand for energy, coupled with thedepletion of fossil fuels and the associated detrimentalenvironmental impact[1].Ethanol is a promising fuel for lowtemperaturedirect fuel cell reactions for itshigh energydensity, low toxicity, ease of storage and availability from different resources [2-6]. In direct ethanol fuel cells (DEFCs), noble metal based materials (Pt, Pdand their alloys) arethe most effective catalystsdue to their superior properties in the adsorption and dissociationof small organic molecules, but the high cost, limitedavailability as well as unsatisfactory cycle life restrict theirpractical applications [2-13]. In recent years, lots of explorations have been made to obtain advanced noble metal-based hetero-structures for improving the performance of DEFCs, such as graphene-supported Pt nanoparticles, free-standing Pd-Au bimetallic nanotube and noble metal membrane [14-22]. Despite all these progress, the catalysts are also noble metal-based. How to develop effective noble metal-free anode catalysts for ethanol electro-oxidationremains a challenging goal.

Layered double hydroxides (LDHs) are a family of layered materialsconsisting of positively charged brucite-type octahedrallayers where the charge-balancing anions and water moleculesoccupy the interlayer space [14-15], which have beenwidely used in the fields of electrochemicalsensors[16], super-capacitors[17]and alkaline secondarybatteries [18], owingto their novel structure and desirable properties. Recently, LDHs have been reportedas promising noble metal-free electrodematerials

RSC Advances Accepted Manuscript

for the electrocatalytic oxidationof alcohol in alkaline medium[14-15, 19]. However, a key challenge for LDHs in the applicationof anode catalysts is to enhance the electrochemical activity by tailoring the structures and properties, such as a well-defined hierarchicalarchitecture with high surface area and suitable pore-size distribution,in which all the electroactive species participates infaradaic redox reaction and a fast mass transport and electrontransfer are guaranteed, and co-catalyst to influence intermediate adsorption-desorption.

Herein, we synthesized Ni-Fe LDH nanosheets and hierarchical Ni-Fe LDH@MnO_2 microspheres by a facile and cost-effective approach for highly efficient ethanol electro-oxidation. Furthermore, it is anticipated to have an essential insight into the synergistic mechanism for electro-catalytic activity enhancing.

Experimental

Ni-Fe LDH synthesis: In a typical synthesis, co-precipitated Ni-Fe LDH was synthesized by simultaneous dropwise addition of 30 mL of 1.0 M $Ni(NO_3)_2$ and 30 mL of 0.5 M $Fe(NO_3)_3$ solutions to 100 mL of 1.5 M Na_2CO_3 solution during constant stirring. The pH was adjusted to ~10 by addition of NaOH solution. Then the vessel was transferred to water bath at 65℃ for 6 hours. Finally the precipitate was filtered, washed with deionized water, and dried in air at 80℃.

Ni-Fe LDH@MnO_2 sphere synthesis: To synthesize the composite electrocatalyst, 200 mg of MnO_2 sphere, prepared according to previous works [5], was dispersed into 100 mLdeionized water and ultra-sonicated for 8 min. Then Ni-Fe LDH was synthesized and coated on the surface of MnO_2 sphere. The composite was

RSC Advances Accepted Manuscript

harvestedand denoted as LDH@MnO_2

Material characterization: Powder X-ray diffraction (XRD) patterns of the as-prepared samples were collected on Smartlab XRD diffractometer using a Cu Ka source, with a scan step of 0.02° and a scan range between 5 and 90°. The morphology of the samples was investigated using a transmission electron microscopy (TEM JEOL JEM-2010 HR-TEM). The accelerating voltage was 200 kV.The specific surface area was measured using the Brumauer-Emmett-Teller (BET) method based on the nitrogen adsorption-desorption isotherm at 77 K on a Micrometritics ASAP2020 sorption analyzer.

Electrochemical characterization: Electrochemical measurements were performed on an electrochemical workstation (CHI 660D, CH Instruments Inc., Shanghai) using a traditional three-electrode mode. Pt plate was used as a counter electrode, Hg/HgO as a reference electrode, and glassy carbon (3 mm in diameter) coated with the as-prepared samples, as a working electrode. The working electrode was fabricated as follows: 4 mg of catalysts was dispersed in 2 mL of ethanol solution and sonicated for 5 min; 10 μL of the suspension was dripped onto the surface of a glassy carbon electrode and dried for 15 min; subsequently 2 μL of 0.5% Nafion solution (Sigma-Aldrich) was coated on the electrode surface and dried for another 5 min. Electrocatalytic oxidation of ethanol on the working electrode was measured in 1.0 M KOH + 1.0 M ethanol solution by cyclic voltammetry in the potential range from 0.2 to 0.7 V. Electrochemical impedance spectra(EIS) were measured at 0.5 V from 100 KHz to 0.01 Hz and the perturbing AC amplitude was 5 mV.Electrical current density

RSC Advances Accepted Manuscript

was calculated by normalizing electrical current on the area of the 3 mm diameter glassy carbon electrode. The chronoamperometry (CA) was conducted at 0.5 V for 3600 s.

Results and discussion

The typical XRD pattern of the as-prepared Ni-Fe LDH is presented in Fig.1(a), showing the characteristic diffraction peaks at 2θ of 11.5, 23.3 and 34.6°corresponding to the (003), (006) and (012) plane reflections of 2D hydrotalcite-like materials, evidencing the formation of LDH particles (JCPSD card No.: 40-0215). As shown in Fig.1(b), all diffraction peaks can be unambiguously assigned to the single-phase γ-MnO_2 (JCPSD card No.: 14-0644). According to the XRD pattern shown in Fig. 1(c), it is found that the LDH@MnO_2 sphere is the phase mixture of γ-MnO_2 and Ni-Fe LDH. There is no new phase generated in the synthesis process.

The TEM image, as shown in Fig. 2 (a), displays MnO_2 particles that are mainly spherical and the diameter of these microspheres is about 1-2 μm.Fig. 2 (b) presents the morphology of Ni-FeLDH and it is apparent to see the nanosheet structure of this as-prepared sample. For LDH@MnO_2, as shown in Fig. 2(c), it holds the spherical morphology of the MnO2 and is coated with Ni-FeLDH nanosheets on its surface.Due to the adsorption of Ni^{2+} and Fe^{3+} on MnO_2 spheres surface, Ni-Fe LDH nanosheetscould cover the MnO_2 sphere uniformly when theprecipitant was added. Furthermore, the heterogeneous interface between MnO_2 and solution could facilitate the nucleation of Fe-Ni LDH. It may be another reason for MnO_2 to be covered

RSC Advances Accepted Manuscript

uniformly with Fe-Ni LDH.

The N_2 adsorption and desorption isotherms shown in Fig. 3(a) and (c)clearly indicate the presence of mesopores in the preparedsamples, classified as type IV as defined by the International Union of Pure and Applied Chemistry (IUPAC). A hysteretic loop between the adsorption and desorption branches can be considered type H4, indicative of slit-like pores in the samples. The sample of Ni-Fe LDH shows a BET surface area of 208.33 m^2 g^{-1}, which is much larger than that of LDH@MnO_2composite (103.47 m^2 g^{-1}).The pore volumes of the as-prepared Ni-Fe LDH and LDH@MnO_2 microsphere are 0.883 and 0.208 cm^3 g^{-1}, respectively. As shown in Fig. 3(b) and (d), the pore size distributions from the adsorption branch of the isotherms using the Barrett-Joyner-Halenda (BJH) method revealthat the pore size of Ni-Fe LDH focuses on 5~30 nm and for LDH@MnO_2, most of the pores have diameters under 20 nm.

The catalytic activities of the as-prepared catalysts towards ethanol electrooxidation were subsequently evaluated in an alkaline medium. The oxidation current was normalized to the electrode surface area; this allowed the current density to be directly used to compare the catalytic activity of different samples. The cyclic voltammograms of ethanol oxidation on the prepared catalysts are shown in Fig. 4. As shown in Fig. 4 (a), the cyclic voltammograms of MnO_2 in alkaline solutions indicate that MnO_2 does not have the catalytic activity to ethanol electro-oxidation. From Fig. 4 (b) and (c), it is seen that the CVs of Ni-Fe LDH and LDH@MnO_2 recorded in 1.0 M KOH solution without ethanol consist of a pair of redox peaks, corresponding to the reversible redox

RSC Advances Accepted Manuscript

of Fe^{2+}/Fe^{3+} associated with OH^-. In the presence of 1.0 M ethanol, both Ni-Fe LDH and LDH@MnO_2 display electrocatalyticbehavior to ethanol oxidation. The onset potentials of the forward anodic peak for both Ni-Fe LDH and LDH@MnO_2 were 0.557 V vs Hg/HgO. Furthermore, as shown in Fig. 4(d), the electrocatalytic behavior to ethanol oxidation is significantly enhanced for LDH@MnO_2 sphere in comparison with Ni-Fe LDH nanosheet. Generally speaking, a larger specific surface area and pore volume can provide more electroactive sites as well as effective diffusion channels for electrolyte ions. In particular, abundant mesopores benefit the mass diffusion and electron transfer, which guarantees highly efficient electrooxidation reaction. However, according to the analysis for nitrogen adsorption isotherms (Fig. 3), though the LDH@MnO_2 sphere possesses a smaller specific surface area and mesopore volume than Ni-Fe LDH nanosheet, but the electrocatalytic activity of the former is remarkably superior to that of the latter. Therefore, the performance improvement of LDH@MnO_2 cannot be attributed to the difference of surface and pore properties.

EIS was further applied to analyze the electrocatalytic performance of Ni-Fe LDH and LDH@MnO_2. Fig. 4(e) represents the EIS plots of Ni-Fe LDH and LDH@MnO_2 at 0.5 V in 1.0 M KOH+1.0 M ethanol solution and the data were analyzed by an equivalent circuit shown in Fig. 4(f). In the equivalent circuit, R_s is the sum of resistance of electrolyte, electrode material and the contact resistance at the interface of the active material/current collector; $Q$is a constant angle element, which represents the double layer capacitance; R_t is the charge transfer resistance; R_c is the resistance of

RSC Advances Accepted Manuscript

intermediate ad-layer and L is the inductance induced by the intermediate. The values of R_s, C, R_t, R_c and L werecalculated from the CNLS fitting of the experimental impedancespectra and their resulting values are listed in Table 1.

According to the fitting results in Table 1, it is apparent to see the resistances for LDH@MnO_2, no matter R_t or R_c, are smaller than those for Ni-Fe LDH. In other words, the former sample has a smaller charge transfer resistance and intermediate ad-layer resistance. Moreover, it is found from the EIS results that mass diffusion is not a key factor for the electrooxidation process and thus both samples may provide effective diffusion channels despite the differences of surface area and pore volume. Additionally, it is well known that the adsorption of OH_{ads}species onto MnO_2 is more favorable [6]. Therefore, it is inferred that MnO_2 could increase the concentration of OH_{ads}species on Ni-Fe LDH surface, and these OH_{ads}can react with C_{1ad} intermediate species to produce CO_2 or water soluble products, releasing the active sites on LDH for further electrochemical reaction [5, 13-15]. This results in a better electrocatalyticperformance in ethanol electro-oxidation process than Ni-Fe LDH. Further investigations of the mechanism are ongoing at our lab.

To evaluate the electrocatalytic activity and stability of Ni-Fe LDH and LDH@MnO_2 composite under continuous operating conditions, CV cycling tests were carried out in a 1.0 M KOH + 1.0 M ethanol solution, as shown in Fig. 4 (g). After 100 potential cycles, 90.8% of the initial catalytic activity was still maintained for LDH@MnO_2 sphere. This is highly superior to the Ni-Fe LDH nanosheet (60.2%), indicating the greatly improved stability of the LDH@MnO_2 sphere. In addition, the

RSC Advances Accepted Manuscript

cycling stability of these two samples was also studied by testing CA curves. Fig. 4 (h) shows the current density curves versus time recorded at 0.5 V for 3600s. It was found that the oxidation current density on the LDH@MnO_2 sphere is much higher than that on Ni-Fe LDH nanosheet over the whole time range, further demonstrating a significantly enhanced electrocatalytic activity. Moreover, this also indicates that the LDH@MnO_2 catalyst possesses good long-term durability for ethanol electro-oxidation in alkaline media.

Conclusions

In this work, Ni-Fe LDH nanosheet and hierarchical Ni-Fe LDH@MnO_2 sphere were synthesized by a facile and cost-effective approach for highly efficient ethanol electro-oxidation. According to the CV curves, it is manifested that MnO_2 has no catalytic activity for ethanol electro-oxidation, and the LDH@MnO_2 microsphere displays excellent catalytic activity and robust durability for ethanol electro-oxidation, compared with the Ni-Fe LDH nanosheet. This can be ascribedto that MnO_2 could increase the concentration of OH_{ads}species on Ni-Fe LDH surface, and these OH_{ads}can react with C_{1ad} intermediate species to produce CO_2 or water soluble products, releasing the active sites on LDH for further electrochemical reaction. It is expected that an effective noble-metal free catalyst for ethanol electro-oxidation could be obtained by tailoring structure and properties of LDHs and their composites.

Acknowledge

The authors are grateful for the financial support by One Hundred Talent Program

RSC Advances Accepted Manuscript

of Chinese Academy of Sciences,Chinese National Programs for High Technology Research and Development (2014AA06A513), as well as by the NSFC (51302264) of China.

Reference

1. Y.L. Wang, D.D. Zhang, W.Peng, L. Liu, M.G. Li, Electrocatalytic oxidation of methanol at Ni-Al layered double hydroxide film modified electrode in alkaline medium, Electrochim. Acta56 (2011) 5754-5758.
2. Y. Wang, T.S. Nguyen, C. Wang, X. Wang, Ethanol electrooxidation on Pt/C catalysts promoted with praseodymium oxide nanorods, Dalton T. (2009) 7606-7609.
3. A.L. Wang, H.Xu, J.X.Feng, L.X. Ding, Y.X. Tong, G.R. Li, Design of Pd/PANI/Pd sandwich-structured nanotube array catalysts with special shape effects and synergistic effects for ethanol electrooxidation, J. Am. Chem. Soc. 135 (2013) 10703-10709.
4. J.D. Cai, Y.Z. Zeng, Y.L. Guo, Copper@palladium-copper core-shell nanospheres as a highly effective electrocatalyst for ethanol electro-oxidation in alkaline media, J. Power Sources 270 (2014) 257-261.
5. Y.L. Wang, D.D. Zhang, M. Tang, S.D. Xu, M.G. Li,Electrocatalysis of gold nanoparticles/layered double hydroxides nanocomposites toward methanol electro-oxidation in alkaline medium, ElectrochimActa 55 (2010) 4045-4049.
6. Y.C. Zhao, L. Zhan, J.N. Tian, S.L. Nie, Z. Ning, MnO_2 modified multi-walled carbon nanotubes supported Pd nanoparticles for methanol electro-oxidation in

RSC Advances Accepted Manuscript

alkaline media, Inter. J. Hydrogen Energ.35 (2010) 10522-10526.

7. C.H. Cui, J.W. Yu, H.H. Li, M.R. Gao, H.W. Liang, S.H. Yu, Remarkable enhancement of electrocatalytic activity by tuning the interface of Pd-Au bimetallic nanoparticle tubes, ACS Nano 5 (2011) 4211-4218.
8. R.Z. Jiang, D.T. Tran, J.P. McChure, D. Chu, A class of (Pd-Ni-P) electrocatalysts for the ethanol oxidation reaction in alkaline media, ACS Catal. 4 (2014) 2577-2586.
9. L.Z. Li, M.X. Chen, G.B. Huang, N. Yang, L. Zhang, H. Wang, Y. Liu, W. Wang, J.P. Gao, A green method to prepare Pd-Ag nanoparticles supported on reduced graphene oxide and their electrochemical catalysis of methanol and ethanol oxidation, J. Power Sources 263 (2014) 13-21.
10. F.F. Ren, H.W. Wang, C.Y. Zhai, M.S. Zhu, R.R. Yue, Y.K. Du, P. Yang, J.K. Xu, W.S. Lu, Clean method for the synthesis of reduced graphene oxide-supported PtPd Alloys with high electrocatalytic activity for ethanol oxidation in alkaline medium, ACS Appl. Mater. Inter.6 (2014) 3607-3614.
11. N.Tian, Z.Y. Zhou, N.F. Yu, L.Y. Wang, S.G. Sun, Direct electrodeposition of TetrahexahedralPdnanocrystalswith high-index facets and high catalytic activity for ethanol electrooxidation, J. Am. Chem. Soc. 132(2010) 7580-7581.
12. X.M. Chen, Z.X. Cai, X. Chen, M. Oyama, Green synthesis of graphene-PtPd alloy nanoparticles with high electrocatalytic performance for ethanol oxidation, J. Mater. Chem. A 2(2014) 315-320.
13. Y.L. Wang, H.Q. Ji, W.Peng, L. Liu, F. Gao, M.G. Li, Gold nanoparticle-coated

RSC Advances Accepted Manuscript

Ni/Al layered double hydroxides on glassy carbon electrode for enhanced methanol electro-oxidation, Inter. J. Hydrogen Energ.37 (2012) 9324-9329.

14. K.Tdanaga, Y. Furukawa, A. Hayashi, M.Tatsumisago, Direct ethanol fuel cell using hydrotalcite clay as a hydroxide ion conductive electrolyte, Adv. Mater.22 (2010) 4401-4404.
15. M.F. Shao, F.Y.Ning, J.W. Zhao, M. Wei, D.G. Evans, X.Duan, Hierarchical layered double hydroxide microspheres with largely enhanced performance for ethanol elecrooxideation, Adv. Funct. Mater. 23 (2013) 3513-3518.
16. L.J. Chen, B. Sun, X.D. Wang, F.M.Qiao, S.Y. Ai, 2D ultrathin nanosheets of Co-Al layered double hydroxides prepared in L-asparagine soulution: enhanced peroxidase-like activity and colorimetric detection of glucose, J. Mater. Chem. B1 (2013) 2268-2274.
17. J.Memon, J.H. Sun, D.L.Meng, W.Z.Ouyang, M.A. Memon, Y. Huang, S.K. Yan, J.X.Geng, Synthesis of graphene/Ni-Al layered double hydroxide nanowires and their application as an electrode material for supercapacitors, J. Mater. Chem. A2 (2014) 5060-5067.
18. B. Yang, Z.H. Yang, R.J. Wang, Z.B.Feng, Silver nanoparticle deposited layered double hydroxide nanosheets as a novel and high-performing anode material for enhanced Ni-Zn secondary batteries, J. Mater. Chem. A2 (2014) 785-791.
19. G. Karim-eezhad, S.Pashazadeh, A.Pashazadeh, Electrocatalyticoxidation of methanol and ethanol by carbon ceramic electrode modified with Ni/Al LDH nanoparticles, Chin. J. Catal. 33 (2012) 1809-1816.

RSC Advances Accepted Manuscript

20. L.M. Yang, Y.H. Tang, S.L. Luo, C.B. Liu, H.J. Song, D.F. Yan, Palladium nanoparticles supported on vertically oriented reduced graphene oxide for methanol electro-oxidation, Chemsuschem7 (2014) 2907-2913.

21. C.B. Liu, H. Zhang, Y.H. Tang, S.L. Luo, Controllable growth of graphene/Cu composite and its nanoarchitecture-dependent electrocatalytic activity to hydrazine oxidation, J. Mater. Chem. A 2 (2014) 4580-4587.

22. L.M. Yang, D.F. Yan, C.B. Liu, H.J. Song, Y.H. Tang, S.L. Luo, M.J. Liu, Vertically oriented reduced graphene oxide supported dealloyed palladium-copper nanoparticles for methanol electrooxidation, J. Power Sources 278 (2015) 725-732.

23. Z.J. Jia. Y. Wang, T. Qi, Pd nanoparticles supported on Mg-Al-CO_3 layered double hydroxide as an effective catalyst for methanol electro-oxidation, RSC Adv. 5 (2015) 62142-62148.

RSC Advances Accepted Manuscript

Figure caption

Fig.1 Fig.1XRD patterns of Ni-Fe LDH (a), MnO_2 (b) and LDH@MnO_2 sphere (c)

Fig. 2 TEM images of the as-prepared samples, (a) MnO_2 sphere; (b) Ni-Fe LDH and (c) LDH@MnO_2

Fig. 3 N_2 adsorption-desorption isotherms of (a) Ni-Fe LDH; (c)LDH@MnO_2 and pore size distribution of (b) Ni-Fe LDH; (d)LDH@MnO_2

Fig. 4 (a-c) The cyclic voltammograms of MnO_2 (a), Ni-Fe LDH (b) and LDH@MnO_2 sphere (c); (d) cyclic voltammogramscomparison of three catalysts;(e) EIS plots of Ni-Fe LDH and LDH@MnO_2 sphere at 0.5 V; (f) the equivalent electrical circuit; (g) potential cycling stability of Ni-Fe LDH and LDH@MnO_2 sphere and (h) CA curves of Ni-Fe LDH and LDH@MnO_2 sphere in 1.0 M KOH+1.0 M ethanolsolution at a potential of 0.5 V at 25℃

RSC Advances Accepted Manuscript

Fig. 1 (a)

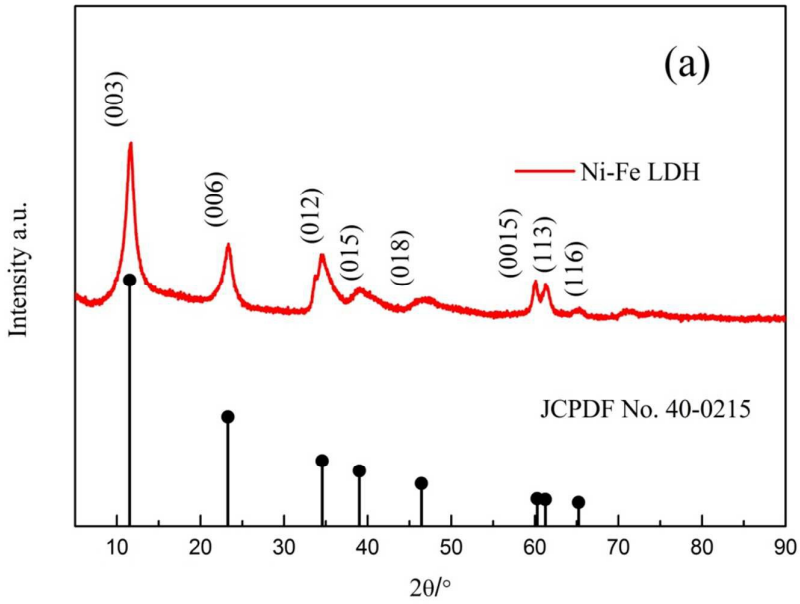

RSC Advances Accepted Manuscript

Fig. 1 (b)

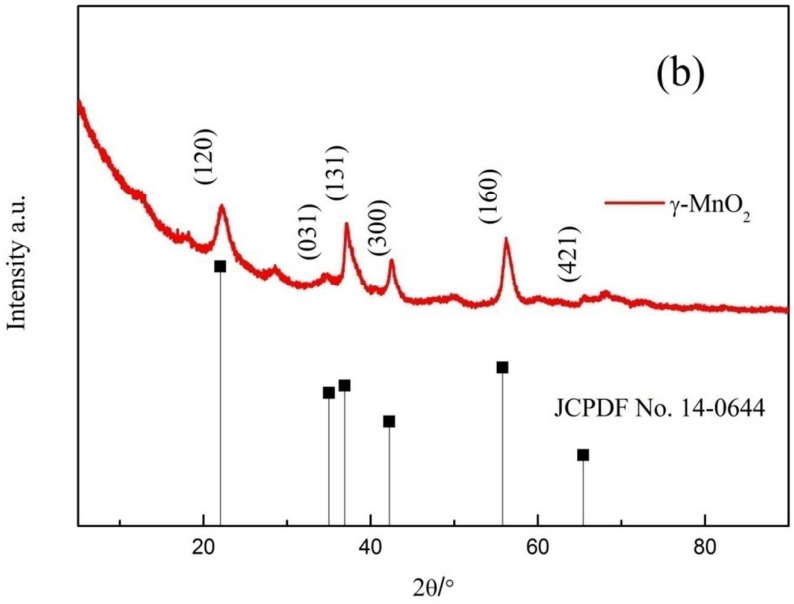

RSC Advances Accepted Manuscript

Fig. 1 (c)

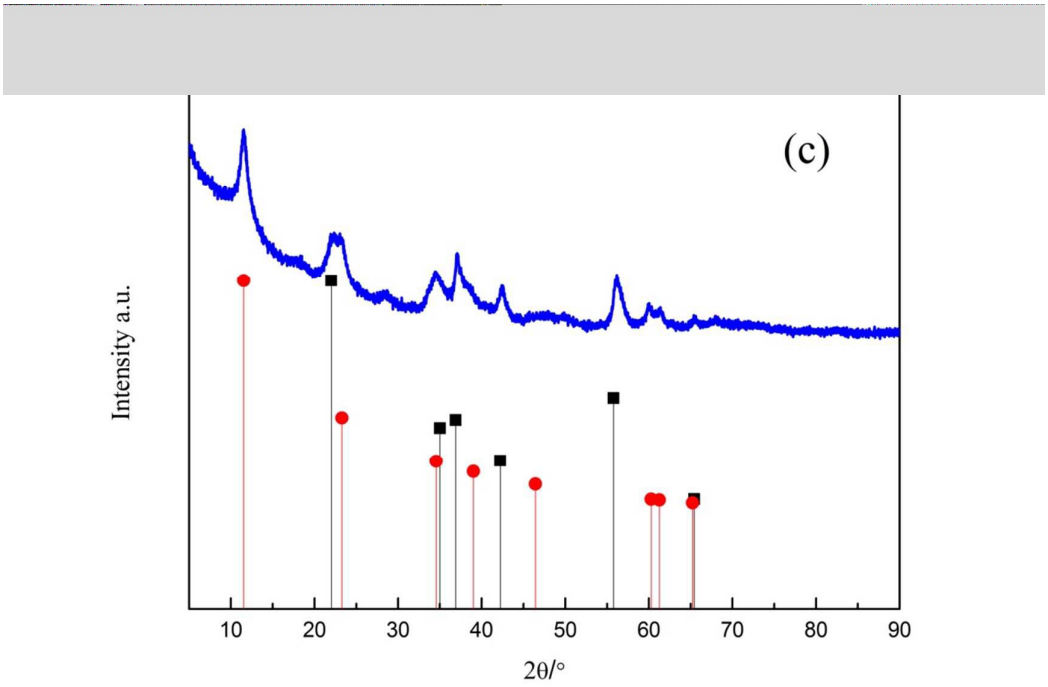

RSC Advances Accepted Manuscript

Fig. 2 (a)

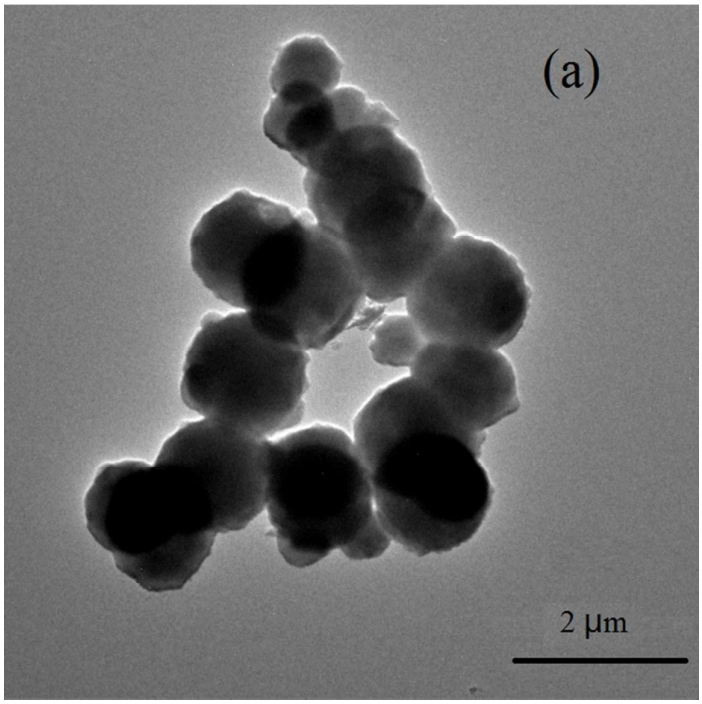

RSC Advances Accepted Manuscript

Fig. 2 (b)

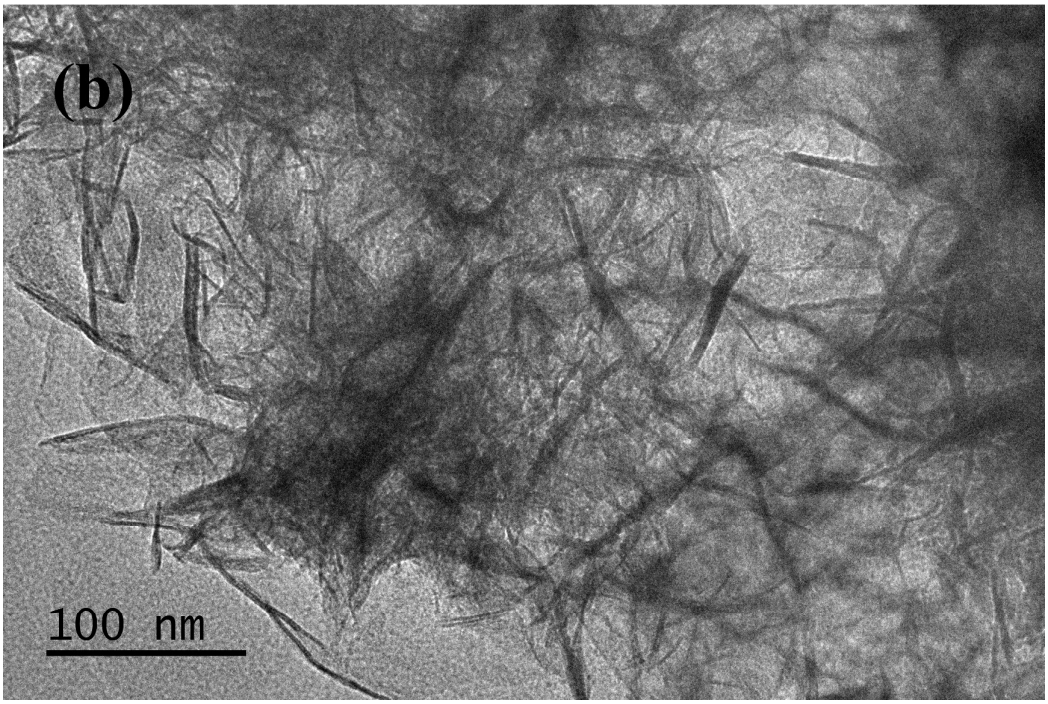

RSC Advances Accepted Manuscript

Fig. 2 (b)

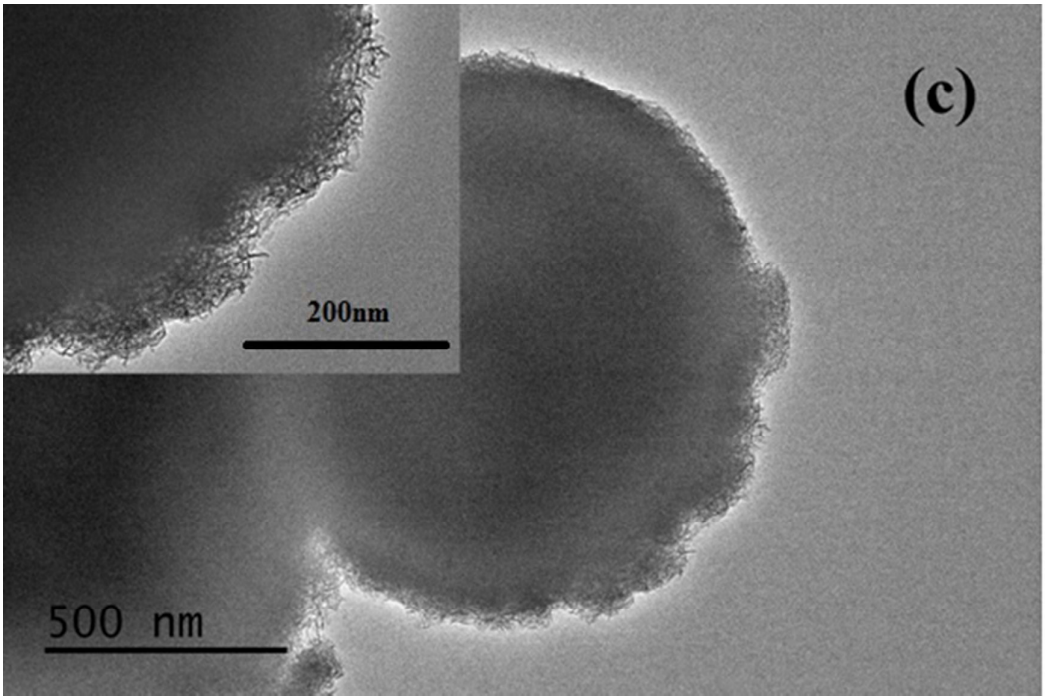

RSC Advances Accepted Manuscript

Fig. 3 (a)

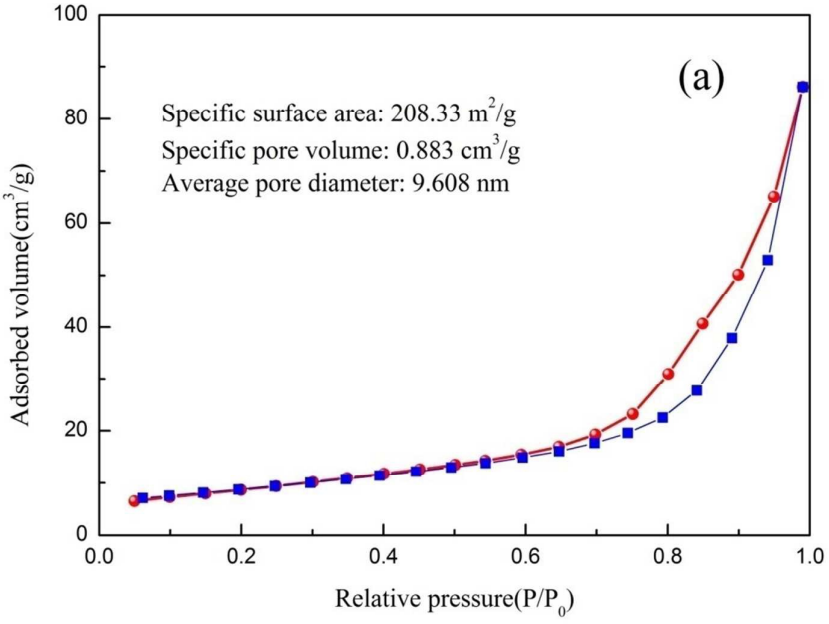

RSC Advances Accepted Manuscript

Fig. 3 (b)

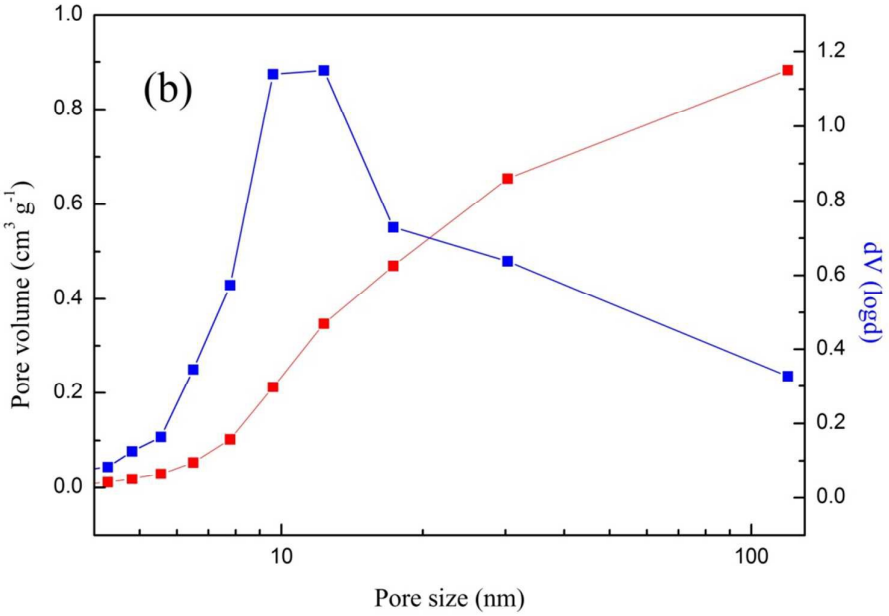

RSC Advances Accepted Manuscript

Fig. 3 (c)

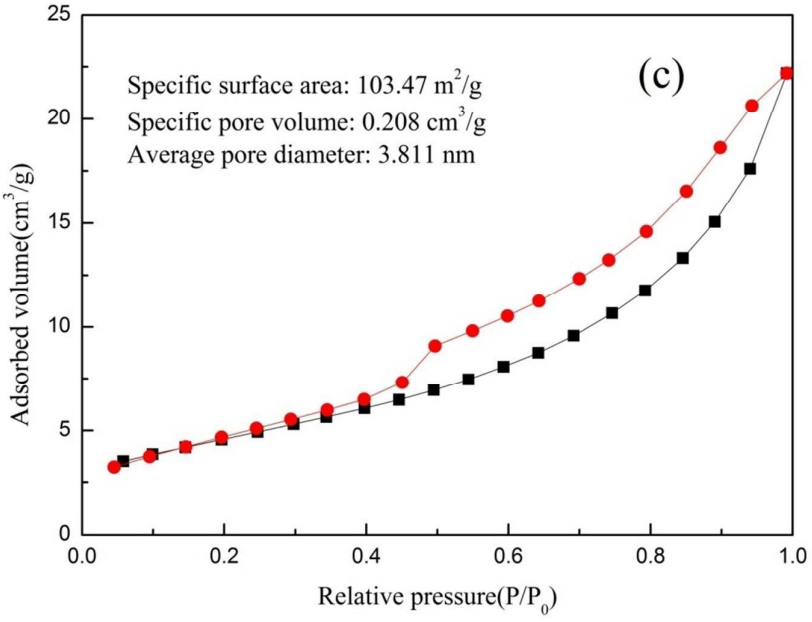

RSC Advances Accepted Manuscript

Fig. 3 (d)

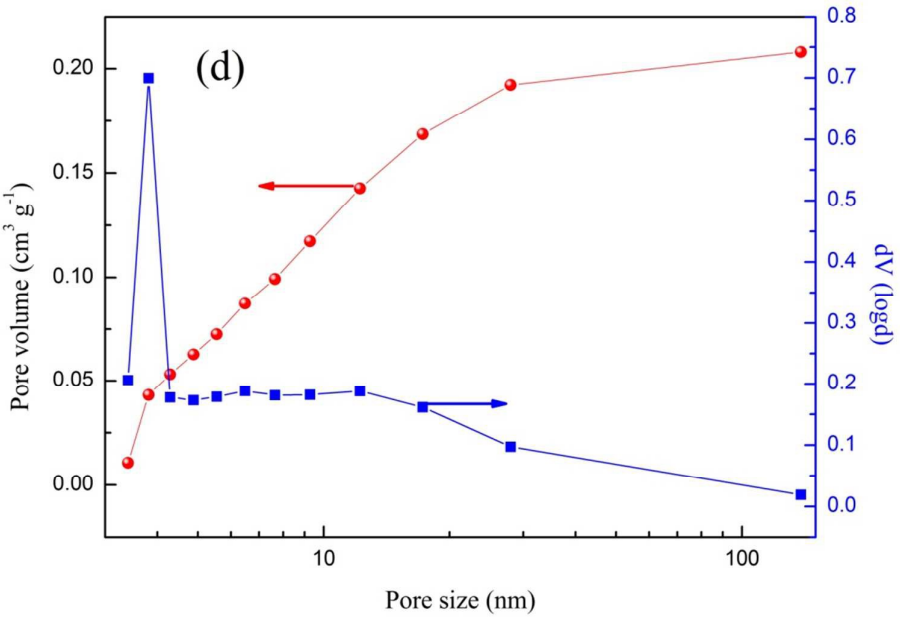

RSC Advances Accepted Manuscript

Fig. 4 (a)

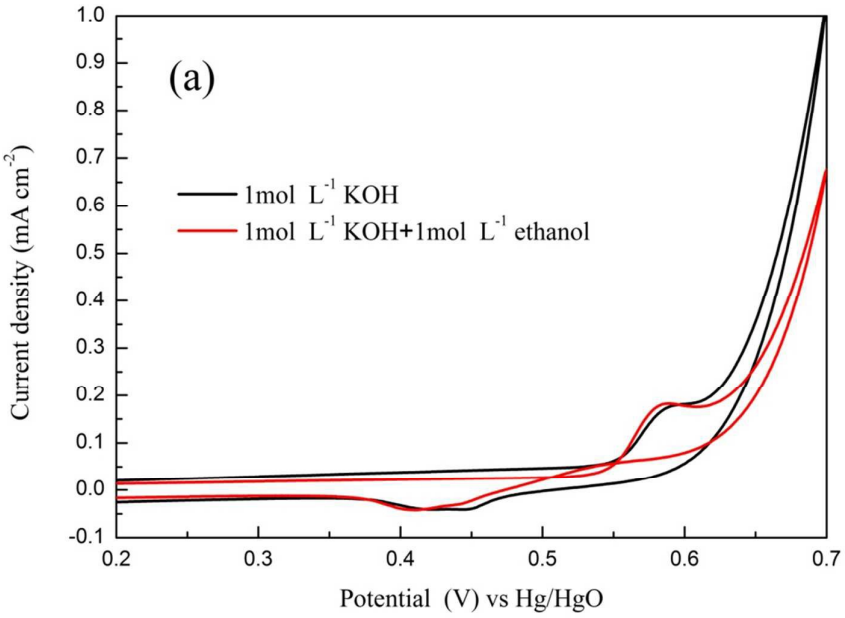

RSC Advances Accepted Manuscript

Fig. 4 (b)

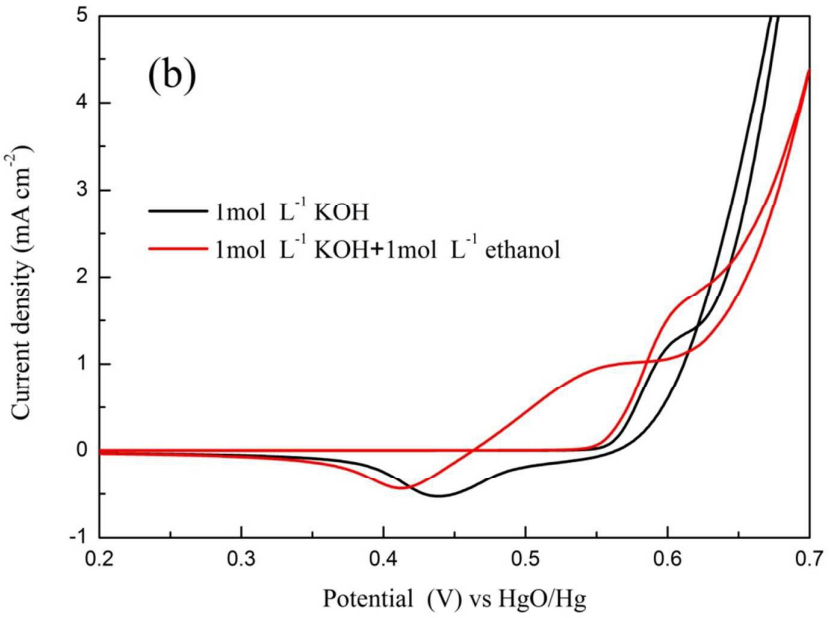

RSC Advances Accepted Manuscript

Fig. 4 (c)

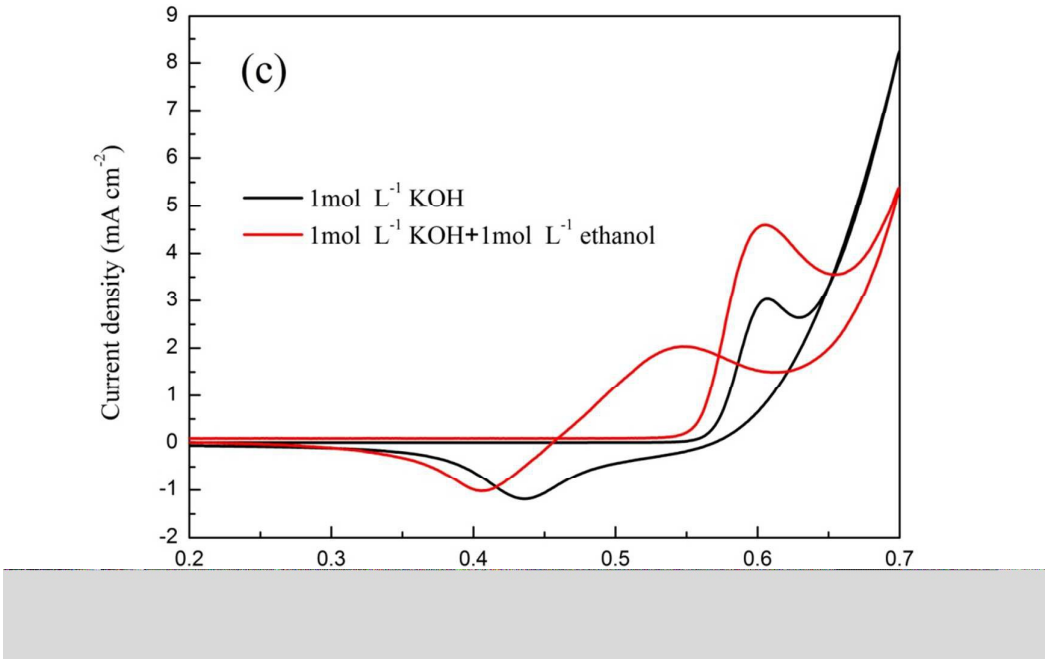

RSC Advances Accepted Manuscript

Fig. 4 (d)

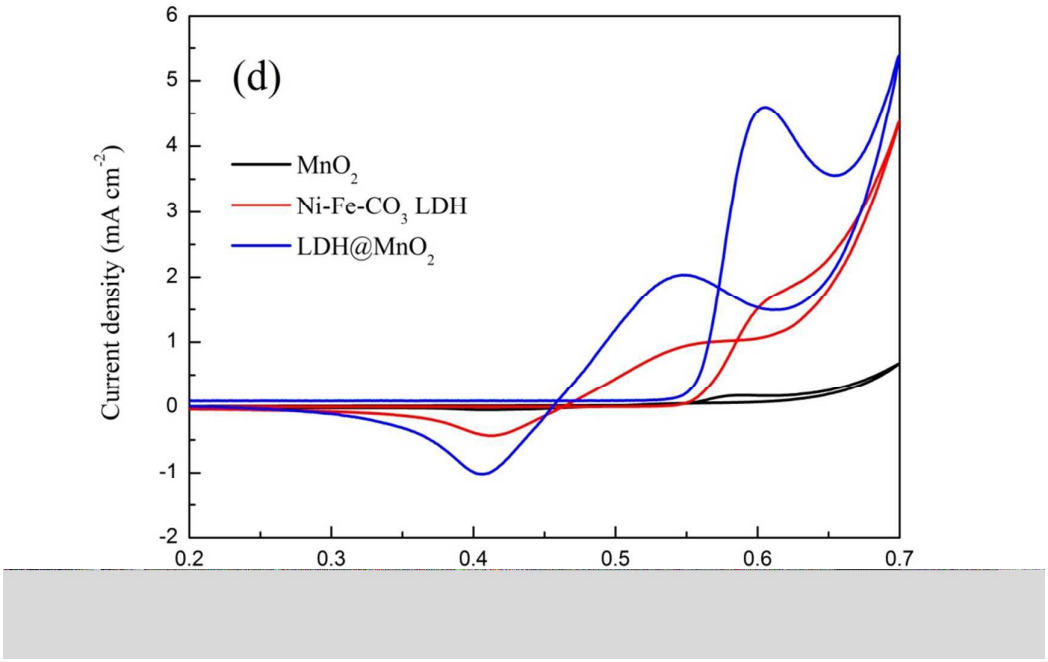

RSC Advances Accepted Manuscript

Fig. 4 (e)

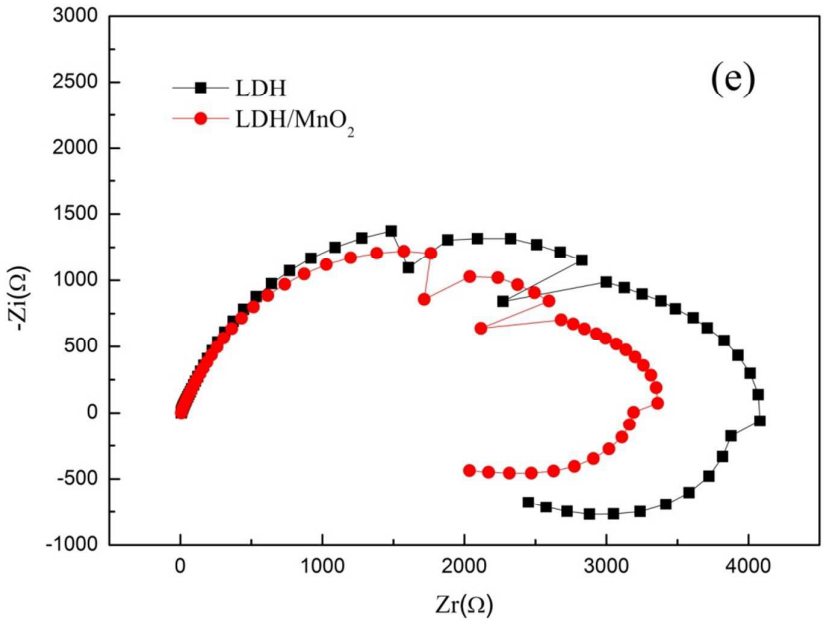

RSC Advances Accepted Manuscript

Fig. 4 (f)

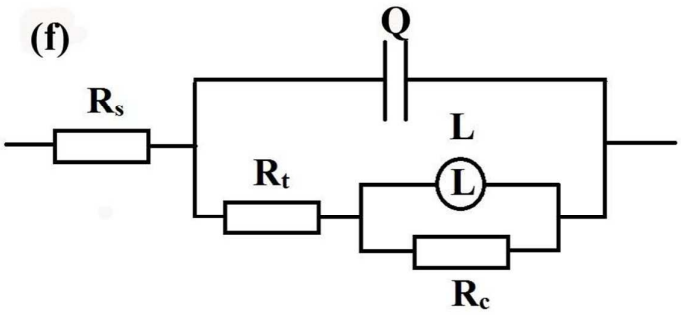

RSC Advances Accepted Manuscript

Fig. 4 (g)

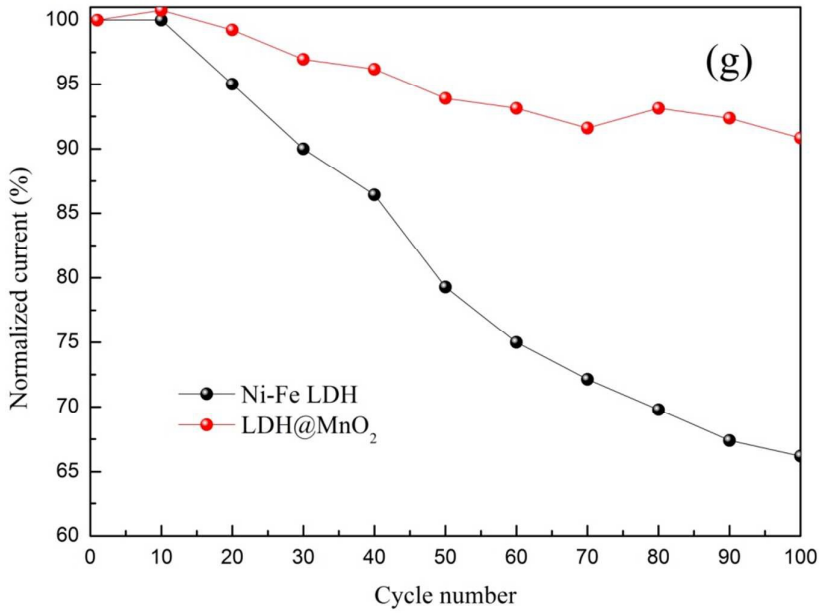

RSC Advances Accepted Manuscript

Fig. 4 (h)

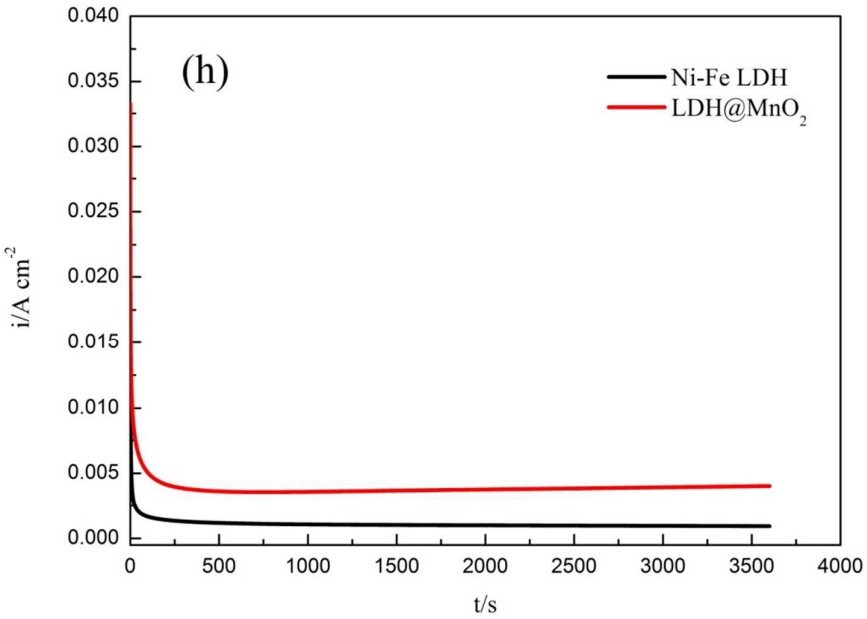

RSC Advances Accepted Manuscript

Figure caption

Table 1 Fitting results of EIS

RSC Advances Accepted Manuscript

Table 1

	R_s(Ω)	Q (Y sec^{-n})	n	R_t(Ω)	R_c(Ω)	L (H)
Ni-Fe LDH	6.149	2.88E-5	0.7833	2157	1747	1.463E4
LDH@MnO_2	6.682	2.523E-5	0.7883	2053	1154	9610

RSC Advances Accepted Manuscript